Reports

Auditory Membrane Vibrations: Measurements at Sub-Angstrom Levels by Optical Heterodyne Spectroscopy

Abstract. *We describe an optical technique for measurement of mechanical vibrations in the auditory organs of living animals. The technique uses light scattered from the vibrating structure and offers several new advantages. Better than 1 angstrom sensitivity, 10 micrometers spatial resolution, and >70 decibels dynamic range are achieved. Illustrative measurements of the mechanical response of the tympanic membrane of crickets* (Gryllidae) *are reported.*

The basis for frequency analysis of complex sounds in the auditory nervous system resides in the mechanical sensitivity of the inner ear. Despite the diversity of receptor organs in both vertebrate and invertebrate species, individual fibers in the auditory nerve universally exhibit frequency selectivity. The basic question is: How do mechanical events in the receptor organ relate to neural tuning? We are studying this question in crickets, where some interesting controversies prevail (*1*).

To facilitate measurements at the level of submicroscopic movements normally encountered in auditory organs, we have developed a technique based on heterodyne detection of scattered laser light that overcomes the limitations of earlier methods (*2*). Our technique permits accurate measurements of vibrational motion at subangstrom amplitudes on surface areas as small as 100 μm^2. No attachment to the organ under study is required. In vivo studies are readily accomplished, since the technique compensates for otherwise prohibitive movements of the living animal.

The essential feature of our method is optical heterodyne detection of the phase modulation of light scattered by the auditory organ as it vibrates at the sound frequency ω_s (*3, 4*). This dictates the design of our optical system (Fig. 1a). In order to mix the scattered light with a reference beam on a photomultiplier cathode for optical heterodyne detection, we use an optical geometry similar to a Michaelson interferometer of small aperture. Coherent light from a helium-neon (HeNe) laser is divided into a reference beam and a probe beam. The probe beam is passed through an optical phase shifter and focused on the vibrating organ. Light that is diffusely backscattered from the organ is imaged onto the photomultiplier, illuminating approximately one coherence area (*4*). The reference beam is reflected onto the same area of the photomultiplier cathode. Small electronically controlled adjustments of the path length of the probe beam are provided by the optical phase shifter.

Periodic phase modulation of the scattered light is introduced by the vibrational motion of the organ. If the electric fields of the reference beam and scattered light mixed at the photocathode are $E_r e^{-i\omega_0 t}$ and $E_s e^{-i(\omega_0 t+\phi)}$, respectively, the photocurrent i will be proportional to

$$|E_r e^{-i\omega_0 t} + E_s e^{-i(\omega_0 t+\phi)}|^2 = E_r^2 + E_s^2 + 2E_r E_s \cos\phi$$

where E_r and E_s are the amplitudes of the two light beams. Here ω_0 is the optical angular frequency ($\sim 10^{15}$ rad/sec) and ϕ is the optical phase difference between the scattered light and reference beam. Therefore, sinusoidal vibrations of the scatterer with amplitude a and angular frequency ω_s yields an optical heterodyne photocurrent (*5*):

$$i = i_s + i_r + 2\epsilon(i_s i_r)^{1/2}\cos[\Omega + (4\pi a/\lambda)\sin\omega_s t]$$

At small vibration amplitudes this simplifies to

$$i \cong i_s + i_r + 2\epsilon(i_s i_r)^{1/2}[\cos\Omega - (4\pi a/\lambda)\sin\Omega\sin\omega_s t + \text{higher harmonics}] \quad (1)$$

$$(a < 400\ \text{Å})$$

where i_s and i_r are the photocurrents for the scattered light and reference beams respectively, ϵ is an efficiency factor ($0 \leq \epsilon \leq 1$) which accounts for coherence area effects and wave-front mismatch of the beams (*4*), Ω is the optical phase difference between the two beams at the photomultiplier when $a=0$ (*6*), and λ is the wavelength of the light. Hence, the signal at ω_s gives the vibrational amplitude of the scatterer.

In order to optimize Ω and provide an absolute calibration for the system, we simultaneously modulate the optical phase shifter at two frequencies, ω_α and ω_β. This introduces several additional terms in the expression for the photomultiplier current; one is proportional to $\sin\Omega\ \sin\omega_\alpha t$, and another is proportional to $\cos\Omega\ \sin\omega_\alpha t\ \sin\omega_\beta t$ (*7*). The first serves as a continuous absolute calibration signal that can be compared with the signal detected at frequency ω_s. The second controls a feedback signal to the phase shifter in order to lock the mean phase at $|\sin\Omega| = 1$ and thereby stabilize the system against movement of the animal subject and drift of the optical apparatus. These provisions are of critical importance in making measurements on living animals, since a change in the position of the scatterer of only $\lambda/8$ (~ 800 Å) can decrease the signal from a maximum ($\sin\Omega = 1$) to zero ($\sin\Omega = 0$).

The circuit used to sort out the various signals (Fig. 1b) employs electronic phase sensitive lock-in detection techniques (*8*). In our experiments the outputs of the two lock-in detectors at ω_s and ω_α are recorded on magnetic tape in the frequency modulation mode for subsequent signal averaging, analysis, and calibration by digital computer.

Scoreboard for Reports: In the past few weeks the editors have received an average of 68 Reports per week and have accepted 12 (17 percent). We plan to accept about 12 reports per week for the next several weeks. In the selection of papers to be published we must deal with several factors: the number of good papers submitted, the number of accepted papers that have not yet been published, the balance of subjects, and length of individual papers.

Authors of Reports published in *Science* find that their results receive good attention from an interdisciplinary audience. Most contributors send us excellent papers that meet high scientific standards. We seek to publish papers on a wide range of subjects, but financial limitations restrict the number of Reports published to about 15 per week. Certain fields are overrepresented. In order to achieve better balance of content, the acceptance rate of items dealing with physical science will be greater than average.

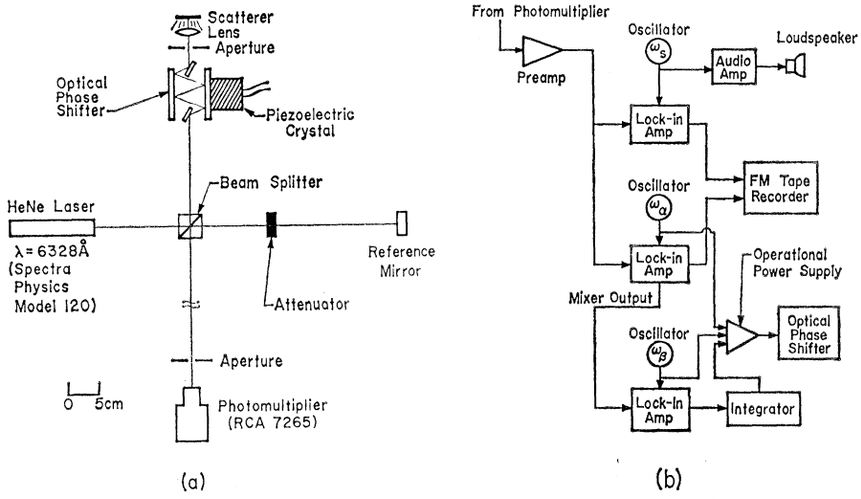

Fig. 1. Measurement apparatus. (a) Optical system, drawn roughly to scale, except that the beam splitter–photomultiplier distance is 75 cm. The focal length of the lens is 3 cm, and the apertures are ~ 1 mm in diameter. The optical phase shifter is based on a Lansing Research Corporation piezoelectric mirror mount. The entire optical system is fastened to a vibration isolation table (Lansing Research Corporation). (b) Electronic system. The lock-in amplifiers are identified in (*8*). The optical phase shifter is driven through a Kepco model OPS2000 operational power supply, and the integrator consists of a Nexus FSK-8 operational amplifier.

On-line analysis is entirely feasible. The feedback control relies on serial detection by the two lock-in amplifiers at ω_α and ω_β to generate an r.m.s. signal that is integrated and fed back to the optical phase shifter.

Our studies of the mechanical response of the auditory organ of living crickets illustrate the features of our system. (Details are in preparation.) We measured the vibrational amplitude of the posterior tympanic membrane (about 0.3 × 0.8 mm and situated on the foreleg) of restrained but not anesthetized crickets in response to tones of various frequencies at constant sound pressure levels in free-field configuration. Figure 2a shows a typical mechanical tuning curve taken on *Gryllus pennsylvanicus* at 90 db SPL (sound pressure level relative to 0.0002 dyne/cm^2). The peak at 5.5 khz corresponds to a similar but sharper peak in the tuning curve recorded from the whole nerve (*9*). Comparable mechanical tuning curves were measured by Johnstone *et al.*, using the Mössbauer effect with a 0.3-μg γ-ray source and a closed sound field (*10*).

We have been able to measure for the first time the linearity of the mechanical response of the tympanic membrane over the entire range of biological interest. Since our optical technique has a dynamic range > 70 db and a sensitivity on the living cricket of 0.1 Å, we have been able to show that the mechanical response of the tympanic membrane is linear over vibration amplitudes from 0.1 to 500 Å for frequencies from 2 to 20 khz. The measurements extend from well below the membrane displacement of 1 Å at neural thresholds to displacements greater than would ever be encountered in the detection of calls of *Gryllidae* (*9*).

Because our optical technique requires no attachment to the membrane, we have also been able to measure the mode structure of the membrane vibration at 5 and 18 khz by simply scanning the membrane with the laser beam. Figure 2b shows the peak displacements at a number of positions on the oval membrane. For both frequencies, the vibrational phase relative to the sound phase was constant over the entire membrane. Therefore, the membrane vibrates in a simple mode at both 5 and 18 khz.

Returning to our measurement technique (*11*), we believe that it is suitable for investigation of the movement of structures within the inner ear, such as the basilar and tectorial membranes in the cochlea (*12*), and for studies of mechanical excitation of sensory hair cells. It could also prove valuable for use on nonbiological mechanical systems at the submicroscopic scale. The instrumental sensitivity (0.05 Å at 10 db signal-to-noise ratio and 3 seconds averaging time), spatial resolution (~ 10 μm), dynamic range (~ 80 db), and tolerance to background movements (velocities up to ~ 1 μm/sec) (*13*) all seem adequate for these applications. Since nothing contacts the vibrating structure, the technique does not perturb normal movement. Only access for the laser beam seems likely to offer a potential problem. Although only conventional acoustic frequency-response measurements are described here, acoustic intermodulation and nonlinear and transient responses are readily determined by appropriate variations of our system.

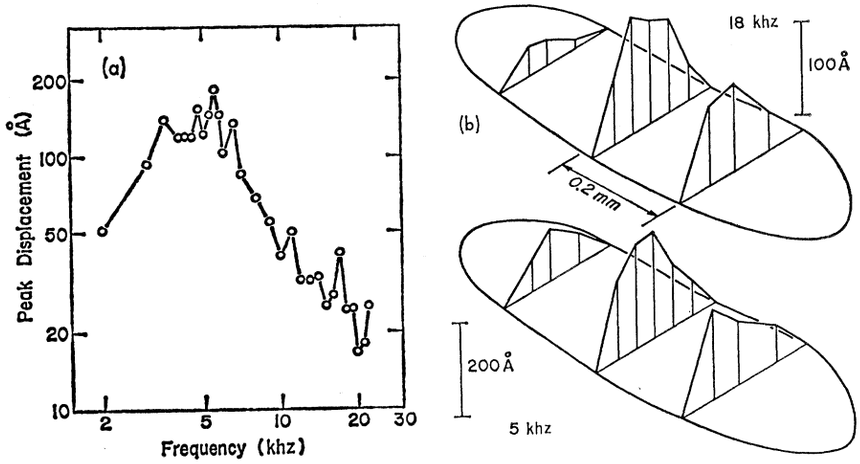

Fig. 2. Mechanical response of the posterior tympanic membrane of *G. pennsylvanicus* to tones at 90 db SPL (relative to 0.0002 dyne/cm^2). (a) Frequency response near the center of the membrane. (b) Peak displacement as a function of position on the membrane.

PAUL R. DRAGSTEN
WATT W. WEBB
School of Applied and Engineering Physics, Cornell University, Ithaca, New York 14850
JOHN A. PATON
ROBERT R. CAPRANICA
School of Electrical Engineering and *Section of Neurobiology and Behavior, Cornell University*

References and Notes

1. J. J. Loftus-Hills, M. J. Littlejohn, K. G. Hill, *Nat. New Biol.* **233**, 184 (1971).
2. Experiments with earlier sensitive methods based on laser interferometry [S. M. Khanna, J. Tonndorf, W. W. Walcott, *J. Acoust. Soc. Am.* **44**, 1555 (1968)] and the Mössbauer effect [P. Gilad, S. Shtrikman, P. Hillman, M. Rubenstein, A. Eviator, *ibid.* **41**, 1232 (1967); B. M. Johnstone and A. J. Boyle, *Science* **158**, 389 (1967); B. M. Johnstone, K. J. Taylor, A. J. Boyle, *J. Acoust. Soc. Am.* **47**, 504 (1970); W. S. Rhode, *ibid.* **49**, 1218 (1971)] have proved to be remarkably fruitful. Both suffer from the need to fasten a foreign object to the organ. The Mössbauer technique requires attachment of a γ-ray source, accumulates data slowly, and works in a narrow dynamic range with frequency dependent sensitivity. The interferometer technique requires attachment and maintenance of alignment of a mirror and is extremely sensitive to small animal movements.
3. For an introduction to this technique, see M. J. French, J. C. Angus, A. G. Walton, *Science* **163**, 345 (1969); and P. Rabinowitz, S. Jacobs, R. Targ, G. Gould, *Proc. I.R.E. (Inst. Radio Engrs.)* **50**, 2365 (1962).
4. H. Z. Cummins and H. L. Swinney, in *Progress in Optics*, E. Wolf, Ed. (North-Holland, Amsterdam, 1970), vol. 8, p. 133.
5. The exact expression is

$$i = i_s + i_r + 2\epsilon(i_s i_r)^{1/2}\{\cos\Omega[J_0(4\pi a/\lambda) + 2\sum_{n=1}^{\infty} J_{2n}(4\pi a/\lambda)\sin(n\omega_s t)] - \sin\Omega[2\sum_{n=0}^{\infty} J_{2n+1}(4\pi a/\lambda)\sin(n\omega_s t)]\}$$

where J_n is the nth order Bessell function. See H. A. Deferrari, R. A. Darby, F. A. Andrews, *J. Acoust. Soc. Am.* **42**, 982 (1967).
6. $\Omega = 4\pi\Delta l/\lambda$, where Δl is the difference in length between the two interferometer arms.
7. The exact expression for the terms discussed in the text is:

$$i = i_s + i_r + 2\epsilon(i_s i_r)^{1/2}[J_0(\alpha)J_0(\beta)J_0(4\pi a/\lambda)\cos\Omega - 2J_1(4\pi a/\lambda)J_0(\alpha)J_0(\beta)\sin\Omega \sin\omega_s t - 2J_1(\alpha)J_0(4\pi a/\lambda)J_0(\beta)\sin\Omega \sin\omega_\alpha t - 4J_1(\alpha)J_1(\beta)J_0(4\pi a/\lambda)\cos\Omega \sin\omega_\alpha t \sin\omega_\beta t + \ldots]$$

where α and β are the phase modulation amplitudes at frequencies ω_α and ω_β, respectively. The zeros of the Bessel functions provide basis for absolute calibration.
8. Our lock-in amplifier at ω_s is a P.A.R. model HR-8, the ω_β lock-in is a P.A.R. model 120, and the ω_α lock-in is an Ithaco model 353. For an introduction to lock-in techniques, see R. D. Moore, *Electronics* **35** (No. 23), 40 (1962); O. C. Chaykowski and R. D. Moore, *Princeton Applied Research Technical Note T-196* (1968) or *Res./Develop.* (April 1968), p. 32.
9. H. Nocke, *J. Comp. Physiol.* **80**, 141 (1972).
10. B. M. Johnstone, J. C. Saunders, J. R. Johnstone, *Nature (Lond.)* **227**, 625 (1970).
11. A detailed publication is in preparation.
12. The scattering properties of these structures should be adequate. We have succeeded in observing the vibration of a translucent internal partition in the cricket trachea. Furthermore, Kohllöffel was able to observe speckle patterns due to scattered lased light from the basilar membrane in the guinea pig cochlea [L. U. E. Kohllöffel, *Acustica* **27**, 49 (1972)].
13. Considerably higher drift velocities can be canceled out by the feedback system alone, but 1 μm/sec has proved to be entirely adequate for our present applications.

14. Research supported by NSF and NIH. We thank J. J. Loftus-Hills for help in the initial phase of this research.

19 March 1974

Woodruffia metabolica: An Exception to the Rule of Desmodexy

Abstract. Woodruffia metabolica *(Protozoa, Ciliophora) has a compound fiber on the left side of its ciliary rows composed of parallel, overlapping ribbons of kinetosome-based microtubules. No similar structure is found connecting the kinetosomes on the right side of the ciliary rows. This arrangement is in opposition to the rule of desmodexy.*

In the ciliated protozoans, one finds some of the most structurally complex cells in existence. Much of this complexity lies in the intricate arrangement of fibrillar systems. Varieties and arrangements of these seem endless but a few common elements have been documented (*1*). One of these, the kinetodesmos, has been known for more than 35 years. As defined by Chatton and Lwoff (*2*), the kinetodesmos is a fiber which connects the kinetosomes (basal bodies) of a ciliary row (kinety); this fiber is always seen accompanying the kinety on its right. It is conventional to refer to the right of a row as if the observer were inside the cell looking outward, with the cell's anterior end uppermost. This constant position of the kinetodesmos led Chatton and Lwoff to propose this orientation as a general feature of many ciliated protozoa, and they termed this generalization desmodexy (*2*). In the subsequent three decades, no exceptions to this generalization were reported; thus, it became known as the rule of desmodexy and has been helpful to electron microscopists for orientation purposes.

The rule of desmodexy has received little challenge in subsequent ultrastructural studies. In 1961 Dumont (*3*) reported an unusual fibrillar arrangement in the proboscis of *Dileptus anser* which, he felt, violated the rule of desmodexy. This apparent exception to the rule cannot be considered valid for two reasons: first, the kinetosomes which give rise to the fiber in question are part of the feeding apparatus (the rule of desmodexy pertains only to body kinetosomes); and, second, the fiber stops short of entering a compound fiber (*4*) and therefore does not connect the kinetosomes in a row. A possible exception to the rule does exist in the ciliate *Colpoda cucullus* (*5*). Here, there is a fiber on the left side of the kineties, but published micrographs do not present a clear picture of the extent of this fiber or whether it connects the kinetosomes in a row. To my knowledge, the arrangement of the newly described fiber in *Woodruffia metabolica* is the first fully demonstrated valid exception to the rule of desmodexy.

Organisms for the study (strain WR1) were fixed for 1 hour in glutaraldehyde in phosphate buffer (2 percent by volume) at *p*H 6.8, postfixed in aqueous osmium tetroxide (2 percent, weight to volume) for 90 minutes, and embedded in an Araldite-Epon mixture (*6*). Flat embedding was employed in order to achieve precise specimen orientation. Thin sections were cut with glass knives on a Porter-Blum MT-2 ultramicrotome, stained with uranyl acetate and lead citrate, and examined with a Hitachi HU-11E electron microscope operated at 75 kv.

Woodruffia metabolica is a large ciliate, frequently measuring 400 μm or more in length (Fig. 1A), flattened ventrally and somewhat flattened dorsally. Viewed from the ventral aspect, its shape varies from an elongate ovoid to somewhat pear-like. The mouth (buccal area) appears as a crescent-shaped slit in the anterior third of the ventral surface. The body has a uniform ciliation arranged in nearly meridional rows originating at the border of the buccal area from which they course posteriad. They are visible in Fig. 1A as dark stripes.

The cell surface shows a series of longitudinal ridges with the cilia arising between them. Kinetosomes of these cilia are always found in pairs; sometimes both kinetosomes bear cilia but often the anterior of the two kinetosomes is barren.

Each kinetosome pair has many of the established fibrillar and microtubular accessories. Figure 2 shows the relationships between the kinetosomes and the fibrillar structures. The orientation of the figure is with anterior to the observer's left and posterior to the right. In Fig. 2, A to D, the views are from inside the cell looking outward and the kinety's left is toward the bottom of the figure; the series shows kinetosome pairs cut at successive levels, with Fig. 2A the most proximal (deepest in the cytoplasm). Figure 2E shows the kinetosome pair in oblique section and Fig. 2F in almost exactly longitudinal section; in both the view is from the left. A postciliary ribbon of microtubules is